scientific reports

Check for updates

OPEN

Magnetic and pH sensitive nanocomposite microspheres for controlled temozolomide delivery in glioblastoma cells

Meysam Ahmadi[1], Muhammad Hossein Ashoub[2], Kamran Heydaryan[3], Sanaz Abolghasemi[4], Elmuez A. Dawi[5], Ghazal khajouei[1]✉ & Mahnaz Amiri[1]✉

Controlled drug delivery systems have been intensively researched for cancer treatment to increase precision targeting and therapeutic efficacy. In this context, novel magnetic-/pH-sensitive graphene oxide/chitosan/iron oxide magnetic nanocomposite microspheres were synthesized. Fe_3O_4 (IO) nanoparticles (NPs) were synthesized via the green synthesis method in the presence of *Salvia officinalis* extract. The graphene oxide (GO) NPs were prepared using the Staudenmaier method, and synthesized materials were characterized. Chitosan (CS) was used to prepare microspheres. GO/CS/IO microspheres were investigated as prospective vehicles for controlled temozolomide delivery in the presence and absence of an external magnetic field. The release percentage of temozolomide molecules in the presence of 100 Hz reached a maximum in 90 min. This is approximately twice the amount of drug release in the absence of a magnetic field and more than that in the presence of a 50 Hz magnetic field. Also, the highest degree of swelling was observed at a pH of 4.5, higher than at a pH of 7.4. Also, the MTT assay results indicated the cytotoxicity of the synthesized microspheres for glioblastoma cells; notably, a significant difference was observed between the groups exposed to the magnetic field and those not, with exposure to the magnetic field further reducing survival. These results indicated that the magnetic microspheres potentially apply to controlled drug delivery systems.

Keywords Glioblastoma, Magnetic Microspheres, PH-sensitive, Temozolomide, Controlled drug delivery

Glioblastoma (GB) is a highly aggressive brain tumor, accounting for about 50% of all gliomas and ranking as the third leading cause of cancer-related mortality[1]. Surgery is the most effective method, but total removal is nearly unattainable due to invasiveness[2]. Treatment options are limited due to tumor heterogeneity, glial stem cell development, invasion, apoptosis, and resistance to radiation and chemotherapy[3,4]. Resection has drawbacks, including potential harm to brain tissue and cognitive function[5]. Physical obstacles in the central nervous system may delay anti-cancer agents[6,7]. Temozolomide (TMZ) is used as GB chemotherapy, causing DNA damage and cell death[8]. However, TMZ, radiation, and surgery are standard therapies, but their effectiveness is limited[9].

Drug delivery involves modifying chemical characteristics like hydrodynamic diameter size, zeta potential, and hydrophobicity to maximize therapeutic effects and minimize adverse effects[10,11]. Conventional methods often cause systemic adverse effects due to rapid drug concentration rise, affecting dosage in blood plasma[12]. Novel drug delivery strategies are needed to reduce systemic drug levels, minimize adverse effects, and achieve controlled drug release in specific regions[13]. Nanomedicine and tailored techniques can enhance the delivery, specificity, and efficacy of new and existing medications for GB patients by addressing the shortcomings of existing treatments[14,15]. Magnetic fields and nanoparticles (NPs) have been used in cancer treatment and drug delivery to accelerate medication accumulation in tumor cells, destroy tissues, and initiate drug release[16]. Recent advancements aim to improve targeting to deep tissues and spatial specificity, with future research focusing on affordable magnetic system technologies and enhanced magnetic particle qualities[17].

[1]Neuroscience Research Center, Institute of Neuropharmacology, Kerman University of Medical Science, Kerman, Iran. [2]Department of Hematology and Medical Laboratory Sciences, Faculty of Allied Medicine, Kerman University of Medical Sciences, Kerman, Iran. [3]Department of Medical Biochemical Analysis, Cihan University-Erbil, Kurdistan Region, Iraq. [4]Department of Microbiology, Faculty of Science, Islamic Azad University, Kerman Branch, Kerman, Iran. [5]Nonlinear Dynamic Research Center (NDRC), College of Humanities and Sciences, Ajman University, P.O. Box 346, Ajman, United Arab Emirates. ✉email: ghazalkhajouei83@gmail.com; mahnazamiri96@yahoo.com

NPs like Fe_3O_4(IO) have become crucial in targeted drug delivery for cancer cells, localized hyperthermia treatment, and MRI[18,19]. However, their instability in aqueous media prevents their standalone use as drug carriers[20]. Coatings using various materials and polymers are applied to address this issue[21,22]. Graphene oxide (GO) nanomaterials have shown potential in regulating the administration of chemotherapeutic medications due to their surface functionalization and toxicity[23–25]. Eco-friendly substances like PEG and chitosan have functionalized GO with safer surface functional groups[26]. Colloidal stability is crucial for secure drug delivery in biological environments[27]. Functionalized GO nanosheets are attractive in medical fields due to their biocompatibility and durability[28,29]. GO's colloidal stability is a potential contender for graphene-based biomaterials, critical in regulating pharmaceutical carrier functionality[30]. Chitosan, a cost-effective, safe, and sustainable material, has been suggested as a potential carrier for pharmaceuticals and biological molecules due to its biological properties[31,32]. However, its tendency to agglomerate magnetic compounds is unsuitable for binding to Fe_3O_4NPs[33]. Therefore, the present work uses graphene oxide (GO) to control the aggregation of magnetic NPs.

Microspheres, spherical particles ranging from 1 to 1000 mm in size, can enhance the bioavailability, stability, and specificity of drugs and proteins[34,35]. They also provide long-term therapeutic benefits by improving solubility and protecting them from enzymatic and photolytic breakdown[36]. In our previous review article, hydrogel microspheres-based nanocomposites in novel drug delivery platforms were investigated in detail[37].

In view of the above, we decided to synthesize novel magnetic-/pH-sensitive graphene oxide/chitosan/iron oxide magnetic nanocomposite microspheres for controlled TMZ delivery in glioblastoma cells. Iron oxide magnetic nanostructures were produced using a green synthesis method in the presence of *Salvia officinalis*extract. Graphene oxide was also prepared using the Staudenmaier method. Furthermore, the release pattern of temozolomide-loaded GO/CS/IO microspheres was examined under both non-magnetic and magnetic field conditions. The cytotoxicity of the synthesized microspheres was evaluated on malignant human glioblastoma cells (A172) and the glioblastoma (T98) cell lines. The schematic representation of the use of a magnetic field for drug release and MTT assay was detailed in our prior work[38]. Figure 1**.** indicates a schematic of magnetic microspheres and drug release under a magnetic field.

Experimental

Materials and methods

Analytical grade compounds were used in the investigation precisely as obtained, without any further purification. Chitosan was procured from Sigma-Aldrich (USA). Other chemical reagents and materials for synthesizing Fe_3O_4 NPs, like $FeCl_2.4H_2O$ and $FeCl_3.6H_2O$, were obtained commercially. Natural graphite flakes, with 99% Carbon and 100 mesh (≥ 80%), were also purchased from Sigma-Aldrich (USA). Fetal bovine serum (FBS) and Dulbecco's modified eagle medium (DMEM) were sourced from Gibco BRL, America. Dimethyl sulfoxide (DMSO) and 3-(4, 5-dimethylthiazol-2-yl)−2, 5-diphenyl tetrazolium bromide (MTT) were bought from Sigma, America. Arshanzist Youtab Company kindly provided Temozolomide (C6H6N6O2).

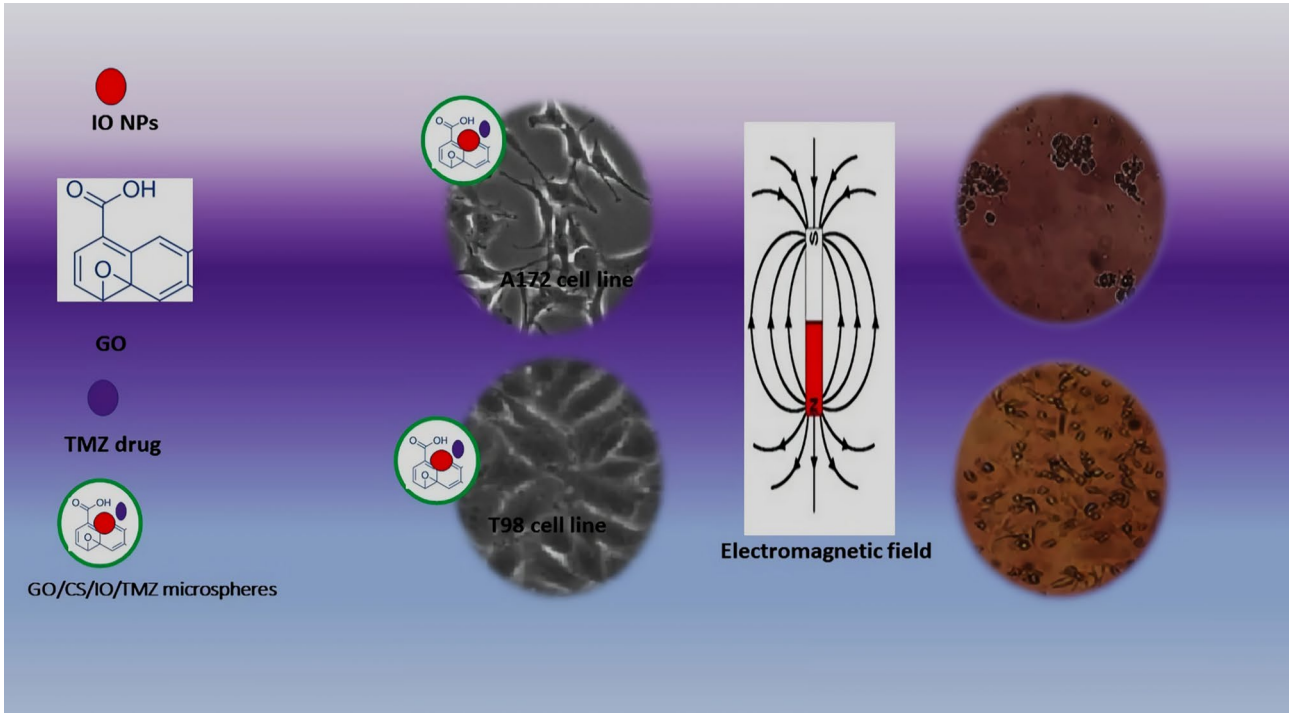

Fig.1. The schematic of magnetic microspheres and drug release under a magnetic field.

Preparation of *Salvia* officinalis

Plants and their components are extensively utilized in research to produce NPs due to their cost-effectiveness and eco-friendly nature. *Salvia officinalis*, a medicinal plant from the Lamiaceae family, is known for its diverse therapeutic properties, including antibacterial, antioxidant, anti-cancer, hypoglycemic, and anti-inflammatory effects[39]. *Salvia Officinalis*has a rich history; its roots, leaves, and stems have been used in traditional medicine for various therapeutic purposes[40]. The plant contains active phytochemicals such as saponins, flavonoid glycosides, phenolic compounds, and multifunctional proteins[41]. The sage leaves were thoroughly cleaned using tap water to remove surface dirt, followed by ultrapure water. Once cleaned, the leaves were dried in a clean, dry, and contaminant-free environment. The dried leaves were then ground into a fine powder, and 10 g of this powder was continuously stirred in 200 mL of deionized water and heated at 60 °C for 2 h. The leaf extract was vacuum filtered, and the resulting solution was stored in a dark and cool place (4 °C) before use.

Iron oxide nanoparticle synthesis

In a standard co-precipitation synthesis, $FeCl_2.4H_2O$ and $FeCl_3$. $6H_2O$ were dissolved in deionized water in a mole ratio of 1:2. This solution was stirred intensively for 2 h at a temperature of 60 °C. Following this, 15 mL of *S. officinalis* leaf extract in aqueous form was added to the mixture of metal salts while stirring continuously. A noticeable color shift in the solution verifies the formation of metallic NPs. Subsequently, the resulting dark brown mixture is centrifugated at 5000 rpm for 20 min to isolate the precipitate from the reaction. The collected solid substance is then rinsed multiple times with deionized water and ethanol. Finally, it was dried at a temperature of 120 °C for 12 h.

Graphite oxide preparation

Graphite Oxide (GO) was produced using the Staudenmaier method[42]. In this process, 1 g of natural flake graphite (45 µm, sourced from Asbury Graphite) was combined with 27 mL of a chilled H2SO4:HNO3 in a 2:1 ratio. The reaction was controlled to stay under 35 ∘C by gradually introducing 11 g of $KClO_3$. After 96 h, 800 mL of ultra-pure (UP) water was incorporated into the solution with continuous stirring, followed by filtration through a 0.45 µm nylon membrane. The resulting Graphene Oxide (GO) precipitate was first washed multiple times with a 5% HCl solution to eliminate sulfate ions (confirmed by the $BaCl_2$ test) and then repeatedly rinsed with UP water to remove chloride ions (verified by the $AgNO_3$ test).

Fabrication of magnetic microspheres

In simple terms, the creation of magnetic chitosan microspheres was achieved through a process known as water-in-oil (W/O) microemulsion polymerization. Initially, chitosan (0.8 g) was completely dissolved in a 2% acetic acid solution (40 mL). Following this, Fe_3O_4 magnetic NPs and GO were uniformly dispersed in the chitosan acetic acid solution using ultrasonic dispersion for half an hour. This solution was then gradually introduced into a microemulsion containing emulsifier (Span-80, 16 mL) and liquid paraffin (320 mL) and was stirred at room temperature for the same duration. Adding a formaldehyde solution (16 mL) was the next step, and it was stirred at a high speed for an hour. As the temperature was increased to 25 ℃, a sodium hydroxide solution (1 mol L^{-1}) was slowly introduced to adjust the pH to a range of 9–10, and the reaction was allowed to proceed for another 4 h. Finally, the resulting black products (GO/CS/IO microspheres) were gathered using a magnet, washed multiple times with petroleum ether, deionized water, and ethanol in that order, and then dried in a vacuum.

The procedure to prepare temozolomide drug-loaded microspheres is as follows. A sample of GO/CS/IO (50 mg) was added to a phosphate buffer solution (PBS, 0.01 mol L^{-1}, 50 mL) that contained TMZ (1.0 mg L^{-1}). This solution was then shaken at 25 ℃ to form uniform loaded microspheres. Various microspheres were prepared as per the details provided in Table 1.

Swelling behavior, drug loading, and in vitro *release*

The method for calculating the loading and release pattern of the sample drug TMZ, which is contained in the magnetically loaded microspheres, is established by the subsequent equation:

$$\text{Drug loading efficiency } (\%) = (\text{Amount of drug in microspheres} / \text{Amount of microspheres}) \times 100$$

UV Visible Spectrophotometer was used to prepare the standard curve of TMZ at a maximum wavelength (ƛmax) of 328 nm in distilled water, slightly varying at ƛmax in other media. The experiments were conducted

Code	chitosan (W/v %)	Fe_3O_4 (W/v %)	GO (W/v %)	Drug (mg/ml %)
BB-1	2	0	0	0
TmzB –1	2	1	2	100
TmzB –2	2	2	2	100
TmzB –3	2	3	2	100
TmzB –4	3	2	2	100
TmzB –5	3	3	2	100

Table 1. Various microsphere formulations.

three times for consistency. The drug loading and in vitro release were examined at different pH levels (4.5 and 7.4). The chosen pH values of 4.5 and 7.4 correspond to the endosomal and physiological pH of cancer cells, respectively. In each experiment, microspheres samples were placed in a dialysis membrane tube (Spectra/Pore, MWCO: 2,000 Da) and dialyzed against 25 mL of water or buffered medium, stirred constantly at 50 rpm. The swelling degree of the magnetic hydrogel microspheres was calculated using a specific formula:

$$\text{Swelling degree } (\%) = (M_s - M_d)/M_d.$$

In this context, M_s and M_d represent the weights of the swollen and dry microspheres, respectively. The pH sensitivity of the microspheres was examined by observing their swelling behavior at pH levels of 4.5 and 7.4. The swelling increased over time, initially quickly and then more slowly, until it reached a constant maximum. The microsphere exhibited maximal swelling behavior (18.8%) under acidic conditions (pH 4.5), surpassing the swelling observed at physiological pH (7.4). Similarly, the drug encapsulation efficiency was significantly enhanced in the acidic environment, reaching 52.2% ± 1% at pH 4.5, which exceeded the values obtained at neutral pH.

The drug release study was conducted by encapsulating 100 mg of drug-loaded magnetic microspheres in a dialysis bag, which was then immersed in buffer solutions (pH 4.5 and 7.4) maintained at 37 °C under constant stirring at 50 rpm. At predetermined intervals, a fixed volume of buffer was extracted and analyzed using UV spectrophotometry at λmax 328 nm to determine the quantity of released drug, comparing against a pre-established standard calibration curve. The extracted volume was replenished with fresh buffer to maintain constant volume. To investigate the effect of magnetic fields on drug release from the magnetic microspheres, the experimental setup described in our previous work was utilized[38].

In vitro *Cytotoxicity*

The T98, A172, and fibroblast L929 cell lines were purchased from the Pasteur Institute's Cell Bank in Tehran, Iran, and cultivated in a standard DMEM medium supplemented with 10% FBS and 1% penicillin/streptomycin. The institute ensured that all requisite tests were performed to validate the cell lines. Detailed information and catalogs of the cell lines can be accessed on the institute's website: https://en.pasteur.ac.ir/Department-of-Cell-Bank. Furthermore, we have consistently received high-quality and satisfactory cell lines from this institution, utilized in several of our published articles[43–47]. The cells were kept at a temperature of 37∘C in a humidified incubator with 5% CO_2. Regular harvesting was done using a solution of trypsin–EDTA (0.25%). The cytotoxicity in vitro was evaluated using a conventional MTT assay from Sigma–Aldrich. The cells were placed into 96-well culture plates at 3×10^4 cells per well and incubated in 5% CO2 at 37∘C for a day. Following this, the medium was substituted with a new one containing microspheres, with or without the TMZ drug, and further incubated for 24 and 48 h, both in the absence and presence of a magnetic field. The MTT assay assessed cell viability compared to the untreated control group.

Characterization of samples

The samples that were synthesized underwent a series of technological characterizations. These included X-ray diffraction (XRD) patterns, which were documented using a Philips-X'pertpro X-ray diffractometer with Ni-filtered Cu Ka radiation. The Fourier transform infrared (FT-IR) spectra were captured using an alpha model FTIR spectrometer from Bruker. Scanning electron microscopy (SEM) images were conducted using the TESCAN MIRA 3 device. The diffuse reflectance of the samples was analyzed using Uv–vis spectroscopy with a Shimadzu UV/3100 in a wavelength range of 200–700 nm. The magnetic properties were assessed using a vibrating sample magnetometer (VSM) model BHV-55 from Riken, Japan. A Metrohm 827 lab pH meter was employed for pH measurements. The optical density (MTT assay) was measured at 490 nm using a Multiskan MK3 microplate reader from Thermo Fisher Scientific, America. Finally, the size distribution and average sizes of the NPs were analyzed using dynamic light scattering (DLS). The VASCO™ nanoparticle size analyzer, manufactured in France, is a specialized instrument designed to characterize nanoparticle suspensions and colloids, utilizing the principles of DLS.

Statistical analysis

Each experiment was conducted a minimum of three times with new samples each time, and the standard deviations were computed from these results. The data was presented as the average ± standard deviation from the trio of experiments. Initially, statistical analysis was performed using a two-way ANOVA test. Subsequently, the significance of the results was assessed through post hoc Tukey's test. A *P*-value of less than 0.05 was considered to indicate statistical significance.

Results and discussion

Characterizations

XRD studies of synthesized samples

The phase and structure of the samples synthesized were examined using XRD measurements, as shown in Fig. 2 **A**. The XRD pattern displayed sharp and intense diffraction peaks corresponding to the (220), (311), (400), (422), (511), and (440) planes. This confirmed the creation of a highly crystalline, single-phase Fe_3O_4nanostructure (JCPDS Card No. 88–0315)[48]. The relatively narrow and high peak shape suggests that the crystals have fully grown and crystallization is complete. The Scherrer equation, expressed as $Dp = 0.9\lambda / (\beta \cos \theta)$, was employed to determine the crystallite size of the nanocrystalline samples. In this formula, Dp represents the crystallite size, 0.9 is the shape factor constant, λ denotes the X-ray wavelength, β is the full width at half maximum (FWHM) of the diffraction peak, and θ is the Bragg angle[49]. Utilizing this equation to analyze the X-ray diffraction data, the

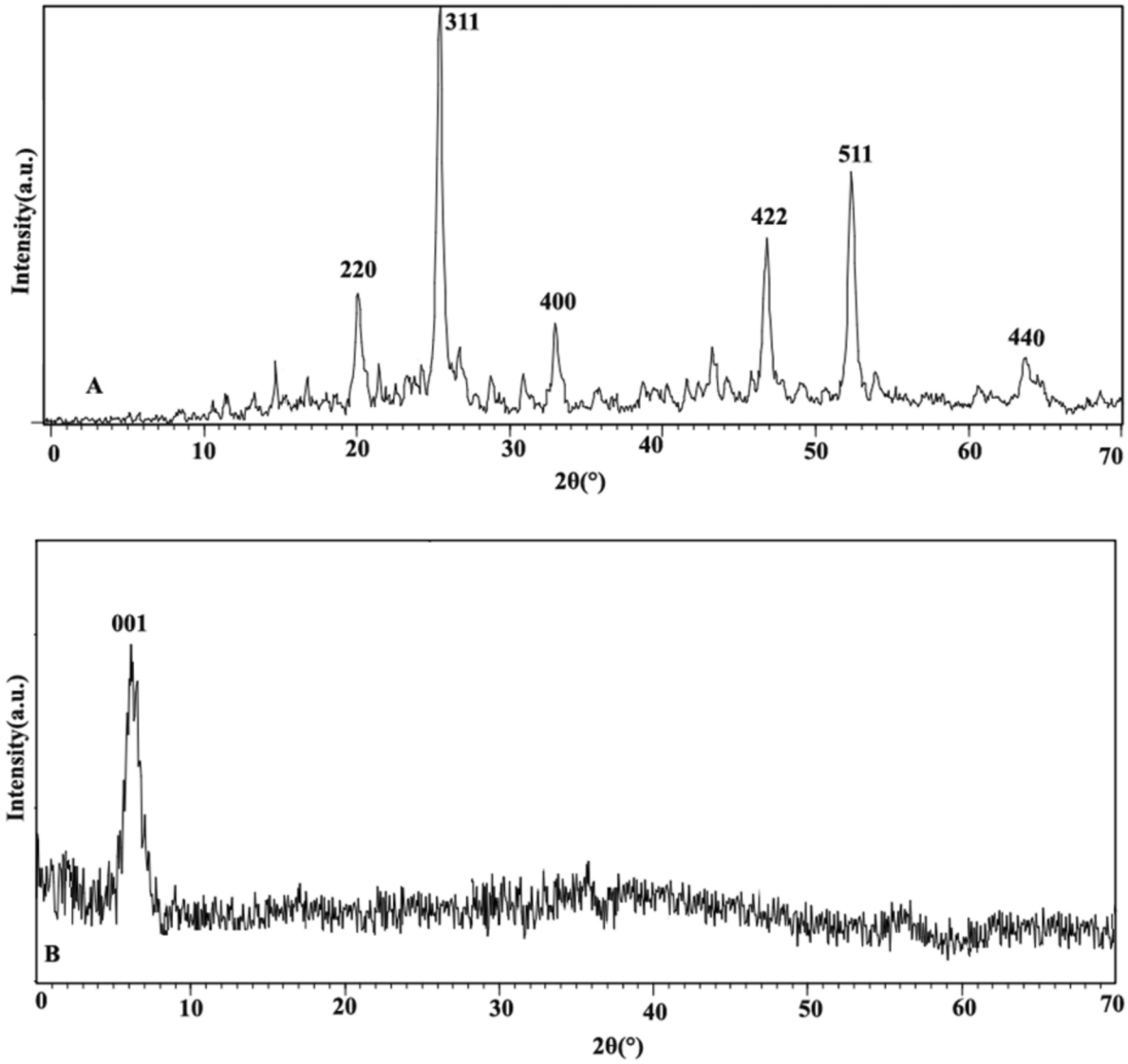

Fig. 2. XRD pattern of (**A**) Fe_3O_4 magnetic NPs and (**B**) GO nanostructures.

average crystallite size of the nanocrystalline samples was calculated to be 24 ± 3.25 nm. Figure 2B displays the XRD pattern of GO. The diffraction peak of exfoliated GO is observed at 2θ = 10.11∘, corresponding to the (001) plane of GO. This indicates the successful transformation of graphite into GO, facilitated by adding oxygen-containing functional groups on the graphene sheets[50].

FTIR analysis

The Fourier Transform Infrared (FTIR) spectrum of Fe_3O_4 NPs dispersed in deionized water is depicted in Fig. 3A. The peak observed at 3414.89 cm^{-1} is attributed to the O–H stretching vibration, which originates from the hydroxyl groups of the water on the NPs. The absorption peaks at 2926.22, 2860.65, 1628.61, 1385.22, and 1020.54 cm^{-1} are associated with the deionized water that was used as a solvent. The absorption peaks at 695.29 and 468.80 cm^{-1} are related to the Fe–O bond vibration of the Fe_3O_4 NPs. These peak values are in close agreement with the values reported by Kim et al.[51].

The GO spectrum exhibits a strong and broad peak at 3417 cm^{-1} (as shown in Fig. 3B), indicating the presence of surface O—H stretching due to the vibrations of the H—O—H groups of water. The other peaks are associated with oxygen functional groups, such as the carboxyl (C O) stretching of COOH groups (1604 cm^{-1}), aromatic (C C) stretching (1404 cm^{-1}), epoxy (C—O) stretching (1071 cm^{-1}), and alkoxy (C—OH) stretching (781 cm^{-1})[52].

The FTIR spectrum of the final sample of magnetic microspheres is shown in Fig. 3C. The image that verifies the fabrication of graphene oxide/chitosan/iron oxide magnetic microspheres shows the peaks associated with the presence of magnetic Fe_3O_4 NPs and GO.

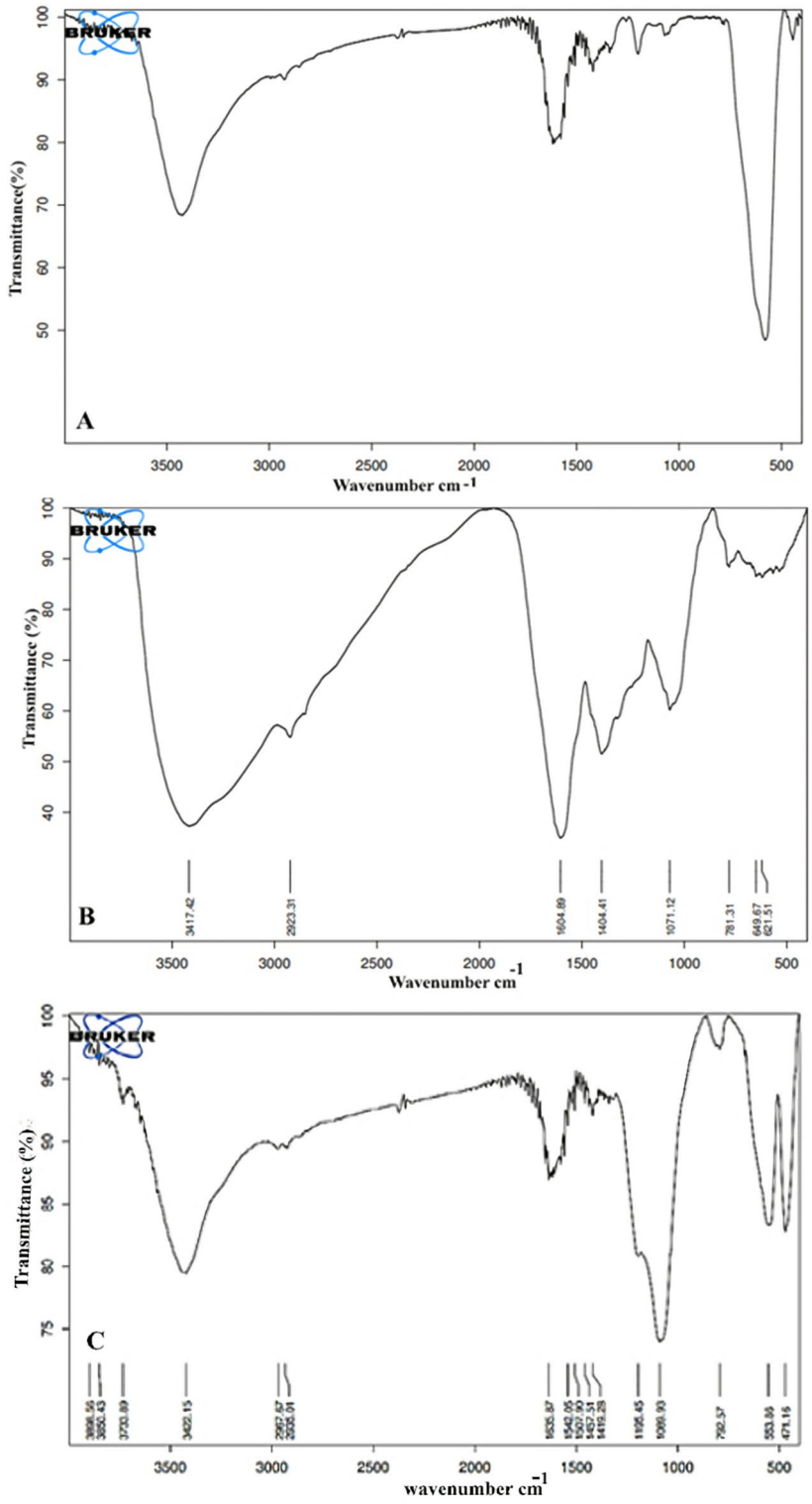

Fig. 3. FTIR pattern of pattern of (A) Fe_3O_4 magnetic NPs and (B) GO nanostructures and (C) the magnetic microspheres.

Magnetic properties investigation

Magnetization assessments were conducted via a Vibrating Sample Magnetometer (VSM) in an air environment at room temperature, with a magnetic field of up to 10 kOe. Figures 4A andB display the magnetic hysteresis loops for IO NPs and microsphere samples. Typically, every sample's loops shift along the positive or negative H axis; this shift is represented by an exchange bias field, which is defined as $HE = (Hc_1 + Hc_2)/2$, with the left coercive field being Hc_1 (<0) and the right coercive field being Hc_2 (>0). In accordance, $Hc = |Hc_1 - Hc_2|/2$ defines

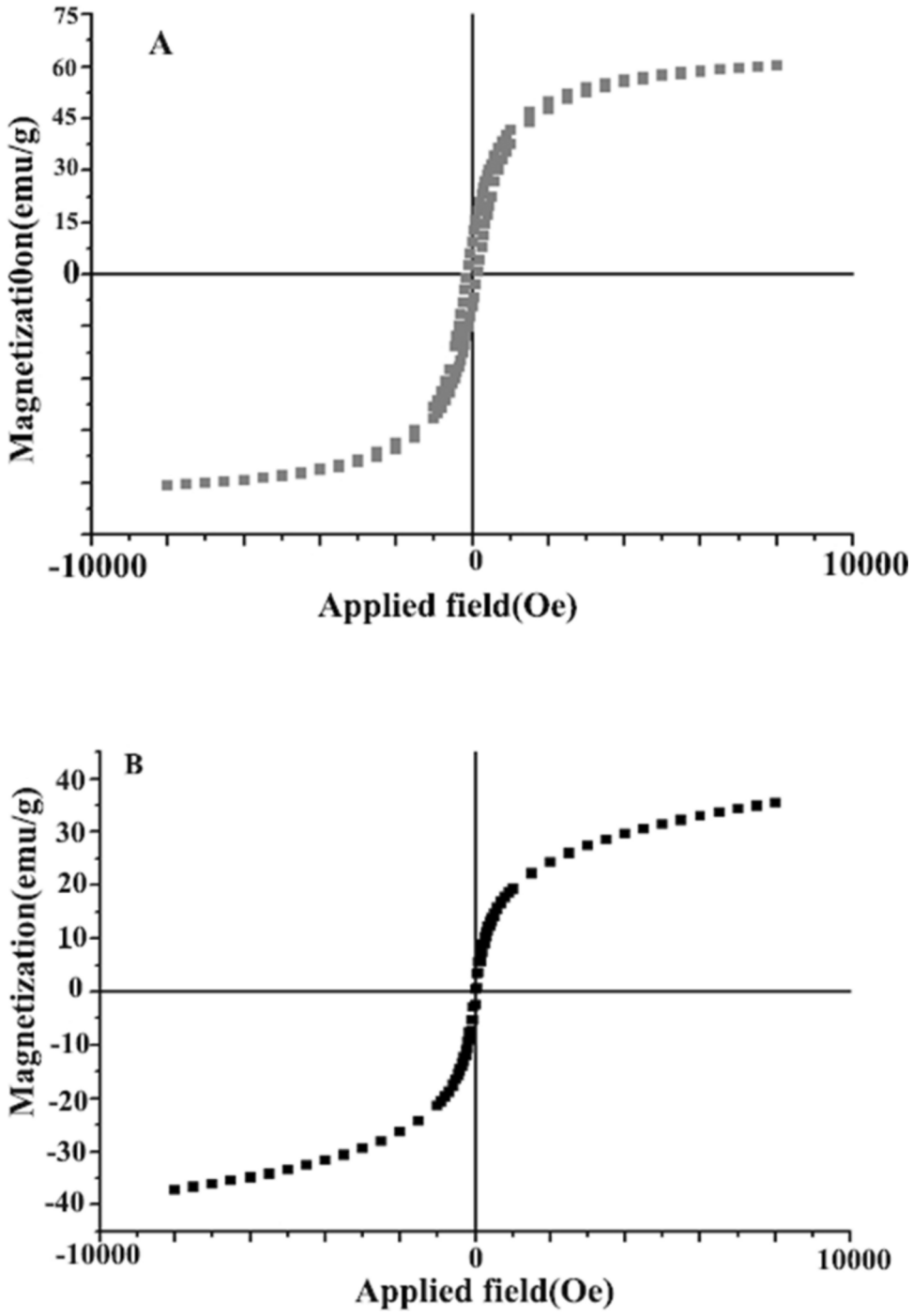

Fig. 4. Magnetic curves of (**A**) Fe_3O_4 magnetic NPs and (**B**) magnetic microspheres.

coercivity[53–55]. The magnetic hysteresis curves see the high magnetic response to a changing magnetic field. Compared to the magnetization of NPs encapsulated in a microsphere, which is about 34.6 emu/g, the saturation magnetization of the IO nanostructure is around 62.4 emu/g. Figures 4C andD show the separation of magnetic NPs after applying an external magnetic field and the microsphere samples' response to the magnet, respectively. The magnetic IO NPs demonstrate an excellent capacity for magnetic guidance. Magnetic microspheres can also be easily moved and collected with an external magnetic field, making them a desirable choice for drug delivery using a remote magnetic field.

SEM, TEM, DLS, and zeta potential analysis

The structure of the magnetic IO NPs and the composite of graphene oxide/chitosan/iron oxide magnetic microspheres were analyzed using scanning electron microscopy (SEM). The SEM images revealed that the IO NPs were spherical, well dispersed, and had a narrow size distribution with an average size of approximately

42.18 ± 1.24 nm. Figure 5B displays the SEM images of the surface of the magnetic microspheres at a higher magnification. Figure 5C indicated the TEM image of magnetic NPs that confirmed that synthesized NPs are in under the 50-nm range of size. Figure 5D presented the SEM image of synthesized GO. The SEM image (Fig. 5D) displayed a wrinkled surface and stacked layered structure. The nano-sized channels between the layers can allow small molecules to pass through, enabling transportation at a molecular scale[56].

Zeta potential and DLS study of magnetic microspheres are shown in Fig. 6. Another crucial factor and helpful metric for determining electronic charge is the zeta potential, which may be utilized to forecast and manage the stability of colloidal suspensions or emulsions[57]. Because charged particles reject one another and thwart the desire to combine, a suspension is more likely to remain stable the higher the zeta potential. It has been demonstrated that microparticles having a zeta potential greater than ± 30 mV are stable in suspension because their surface charge keeps them from aggregating[58]. According to the results, the synthesized microspheres had a zeta potential of around + 45 mV, which was consistent with their high stability and lack of aggregation in the suspension. The strong positive zeta potential suggested that the electrostatic repulsion between particles prevented aggregation and promoted stability. The positive value of the zeta potential may have resulted from the positive charge of chitosan. The biopharmaceutical characteristics of microspheres, their biodistribution, and the absorption of microsphere content can all be influenced by size[59]. By using DLS analysis, the microspheres' size was found to be 623.99 nm.

Drug loading, drug release and swelling behaviors

Figure 7A shows the drug loading efficiency of the samples at two different pH levels. The drug loading percentage at pH 4.5 was 52.2 ± 1, higher than at pH 7.4. Figure 7B illustrates the swelling characteristics of the samples. The swelling increases over time, initially quickly and then more slowly, until it reaches a steady

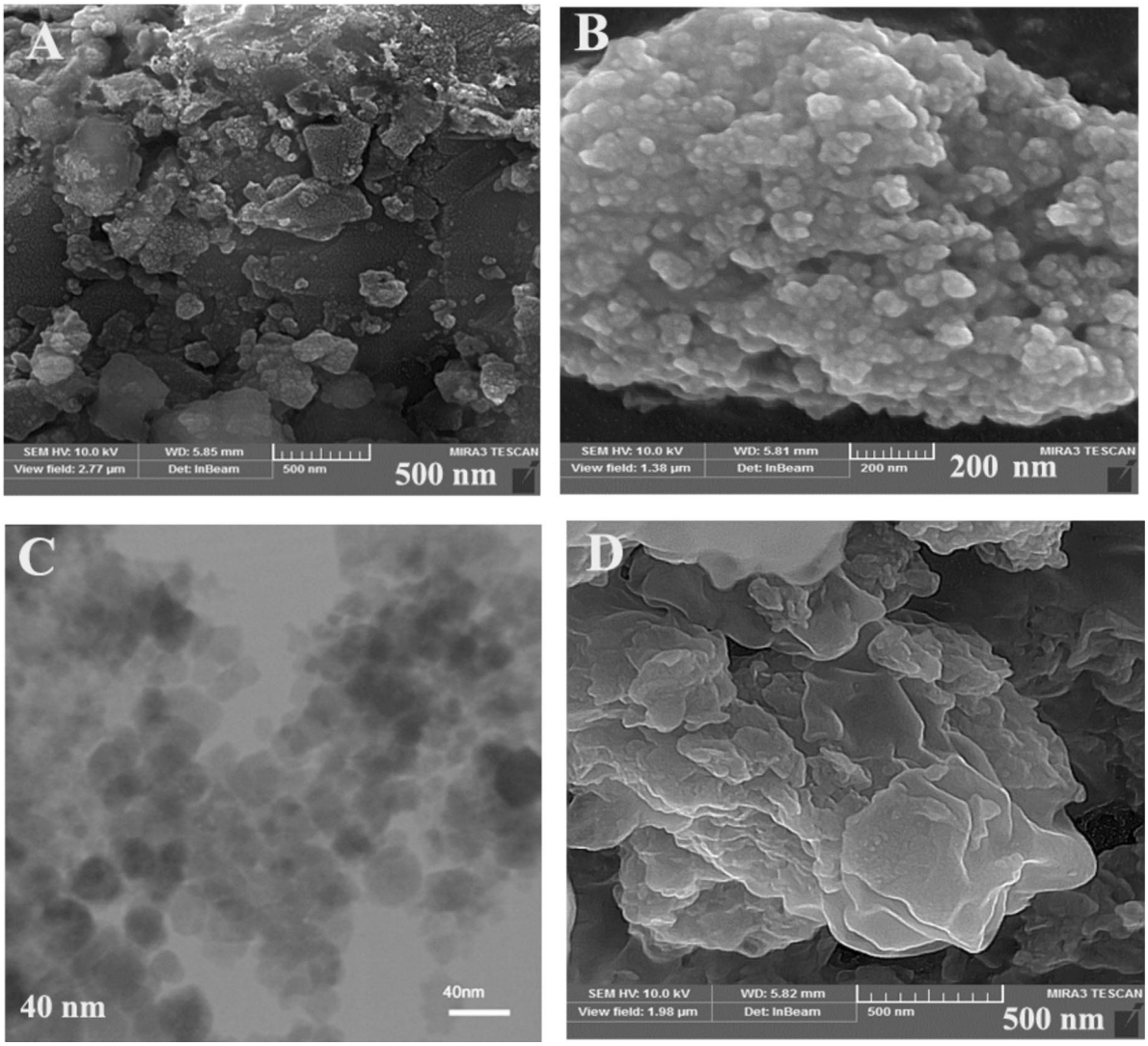

Fig. 5. SEM micrographs of the pattern of (**A**, **B**) Fe_3O_4 magnetic NPs at two magnifications (**C**) TEM image of Fe_3O_4 magnetic NPs and (**D**) SEM of GO nanostructures.

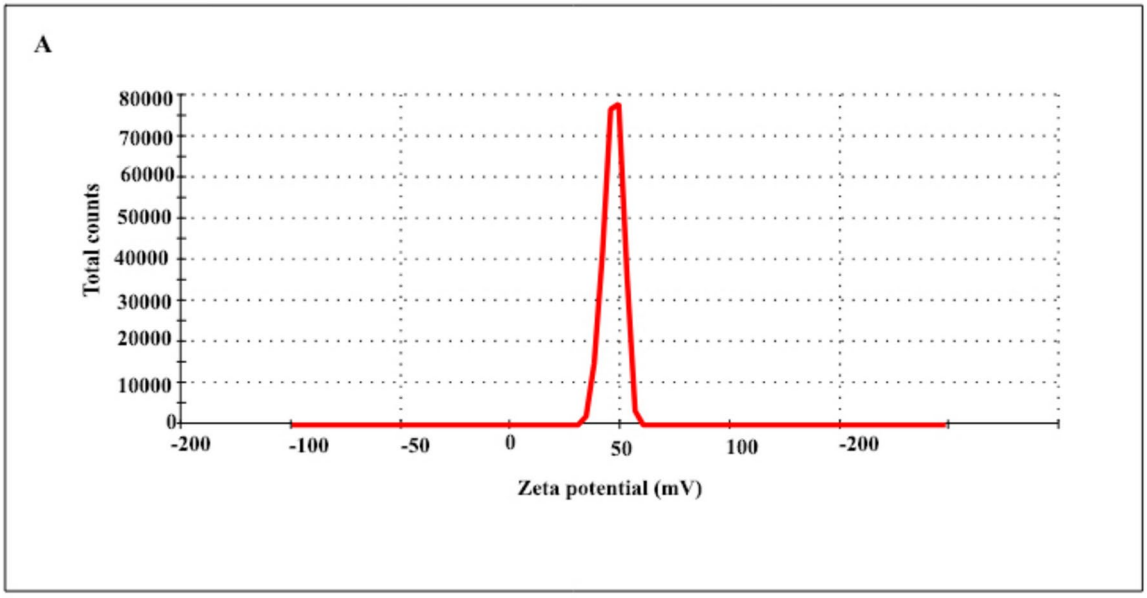

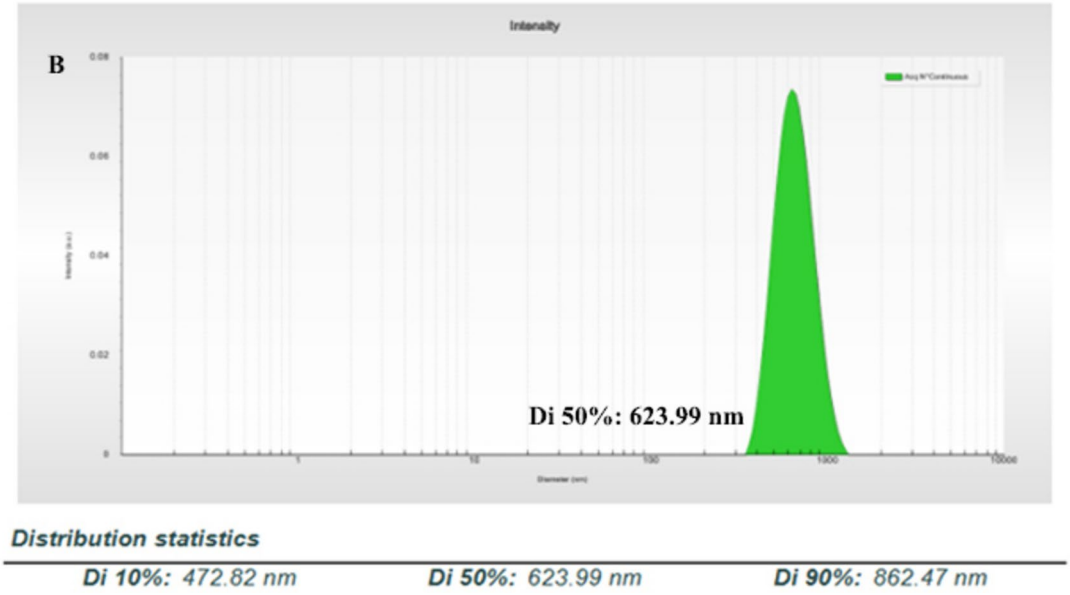

Fig. 6. Zeta potential (**A**) and DLS analysis (**B**) of magnetic microspheres.

maximum. The highest degree of swelling, 18.8%, was observed at a pH of 4.5, which was higher than at a pH of 7.4. There was a significant difference ($P<0.05$) in the swelling and loading rates at pH 7.4 and 4.5. According to this, pH-sensitive hydrogels are practical delivery systems for the targeted release of TMZ, as the environment's pH may be changed to control the drug's release. Due to the superior loading capacity of TmzB-5, these samples were chosen for further investigation on release tests at pH 4.5. The release profile of the TMZ drug from the drug-loaded microspheres Tmz-5 in the presence of 50 and 100 Hz of AC magnetic field at pH 4.5 and 37° C is shown in Fig. 7C. It is clear that the release percentage of TMZ molecules in the presence of 100 Hz reached a maximum of about 52.2% in 90 min. This is twice the amount of drug release in the absence of a magnetic field and more than that in the presence of a 50 Hz magnetic field. When an AC field was applied, the oscillation of the microspheres significantly increased, and release occurred uniformly across the entire area. Particles oscillate at higher AC field frequencies due to frictional interactions with nearby particles, which results in some release. Friction between aligned particles and oscillating NPs in fluid microspheres is responsible for this material's releasing characteristic[60].

In vitro cytotoxicity of GO/CS/IO/TMZ microspheres

Microspheres encapsulate drugs and proteins, improving bioavailability, stability, specificity, and long-term therapeutic benefits by improving solubility and shielding them from enzymatic and photolytic breakdown[61,62].

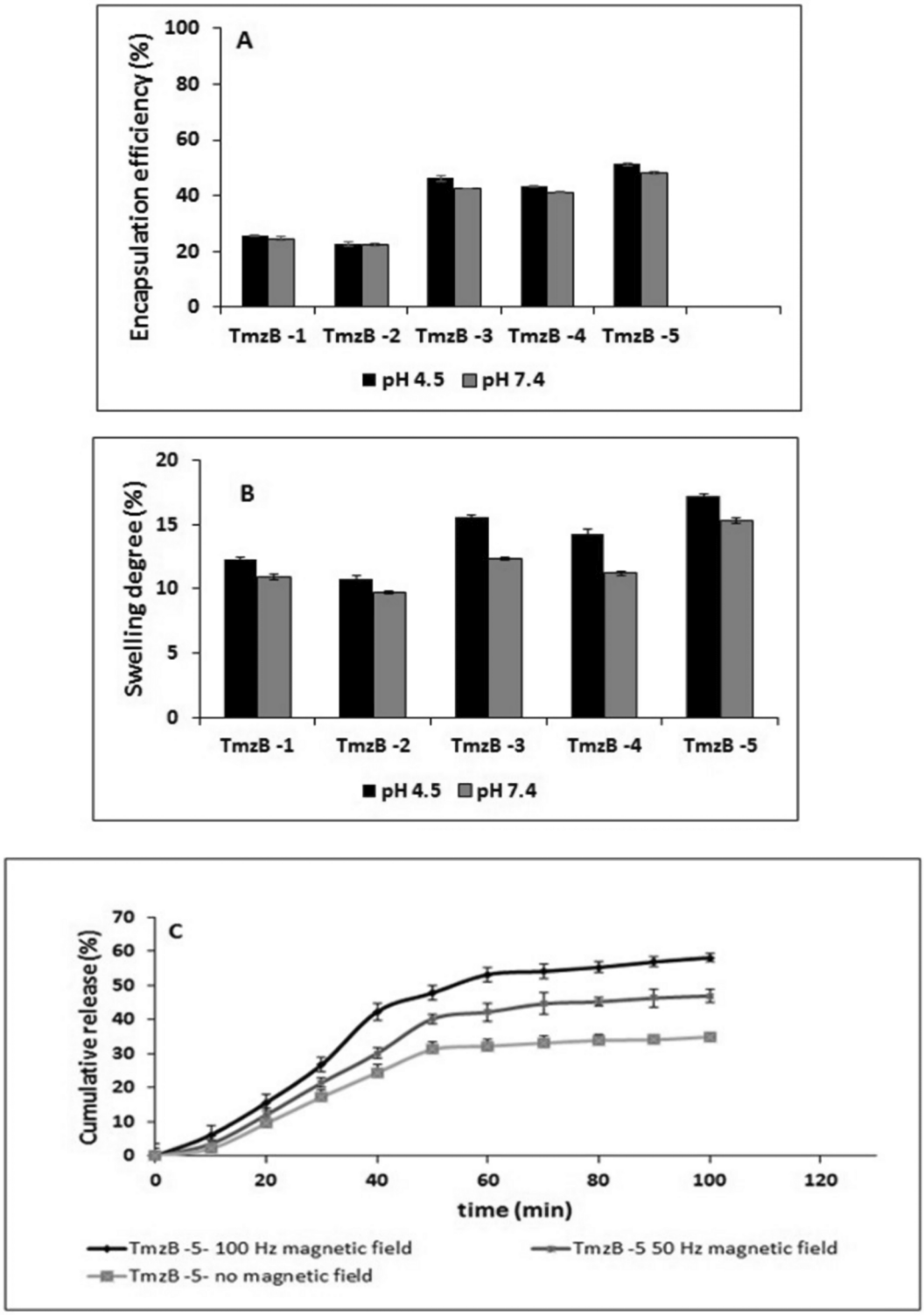

Fig. 7. Drug loading efficiency (**A**) Swelling characteristics (**B**) and Drug release of magnetic microspheres at various magnetic frequencies (**C**).

Biodegradable and synthetic polymeric microspheres are medication delivery systems for malignancies such as colon and GB[63]. In this context, MTT assay was employed to assess the cytotoxic effects of magnetic microspheres on T98, A172, and fibroblast L929 cell lines. As depicted in Figs. 8andFigs. 10(a-c), The viability of A172 cells at 24- and 48-h post-exposure to GO/CS/IO magnetic microspheres is significantly compromised in the presence and absence of a magnetic field when compared to the untreated control group ($P < 0.05$ for 24 h and $P < 0.01$ for 48 h). Furthermore, the proximity of temozolomide-loaded GO/CS/IO magnetic microspheres in the absence of

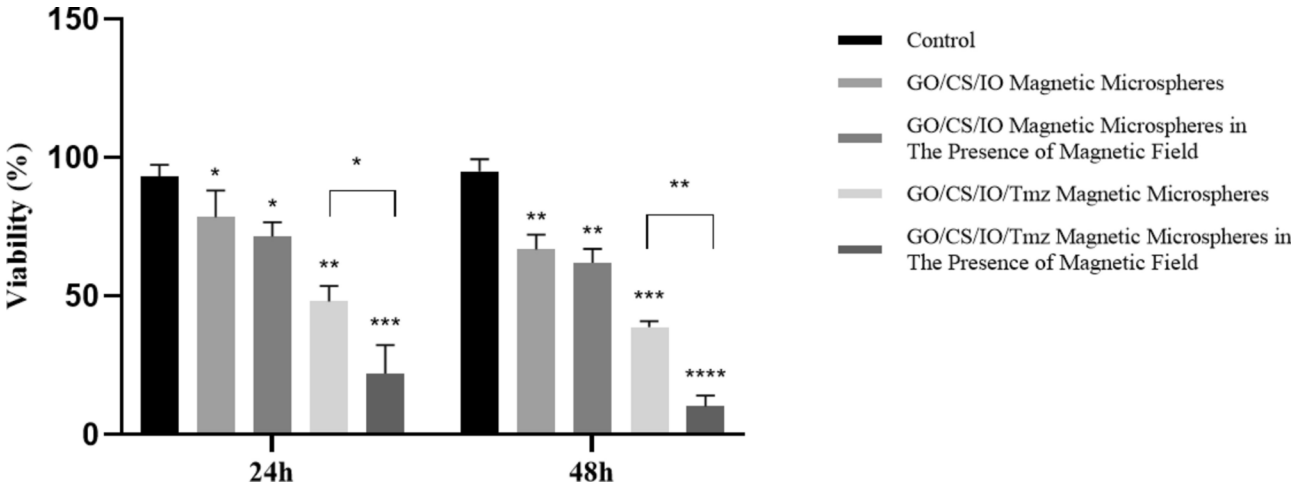

Fig. 8. In vitro cell viability of A172 cell line incubated with (**a**) GO/CS/IO magnetic microspheres, (**b**) GO/CS/IO magnetic microspheres in the presence of magnetic field, (**c**) GO/CS/IO/TMZ magnetic microspheres, (**d**) GO/CS/IO/TMZ magnetic microspheres in the presence of magnetic field, for 24 h (SD ± 2%) and 48 h. $^{*}P < 0.05$, $^{**}P < 0.01$, $^{***}P < 0.001$, $^{****}P < 0.0001$.

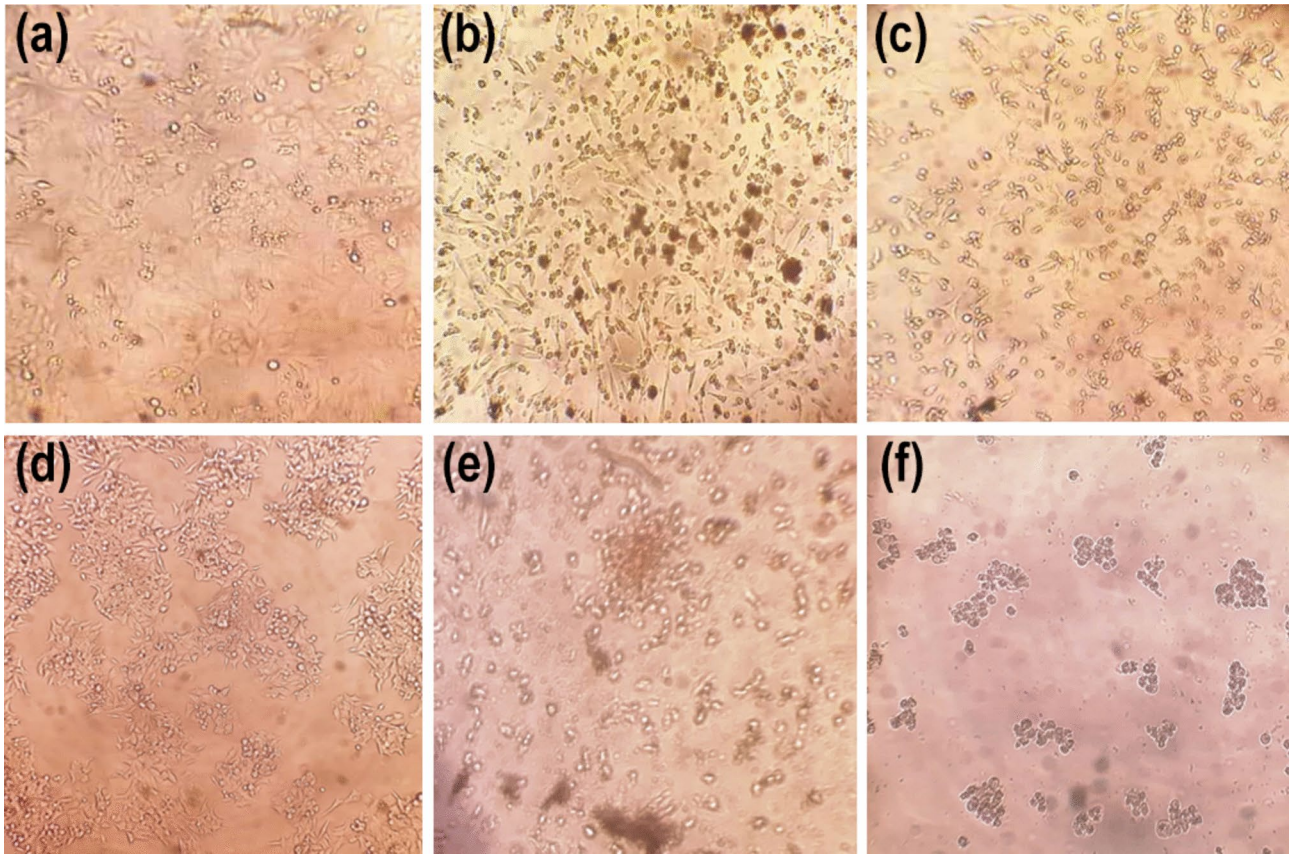

Fig. 10. Optical micrograph (magnification 200×) of T98 cell line treated with GO/CS/IO magnetic microspheres containing TMZ in the absence (**b**) and presence (**c**) of the magnetic field after 24 h compared to untreated control (**a**). Optical micrograph (magnification 200×) of A172 cell line treated with GO/CS/IO magnetic microspheres containing TMZ in the absence (**e**) and presence (**f**) of the magnetic field after 24 h compared to untreated control (**d**).

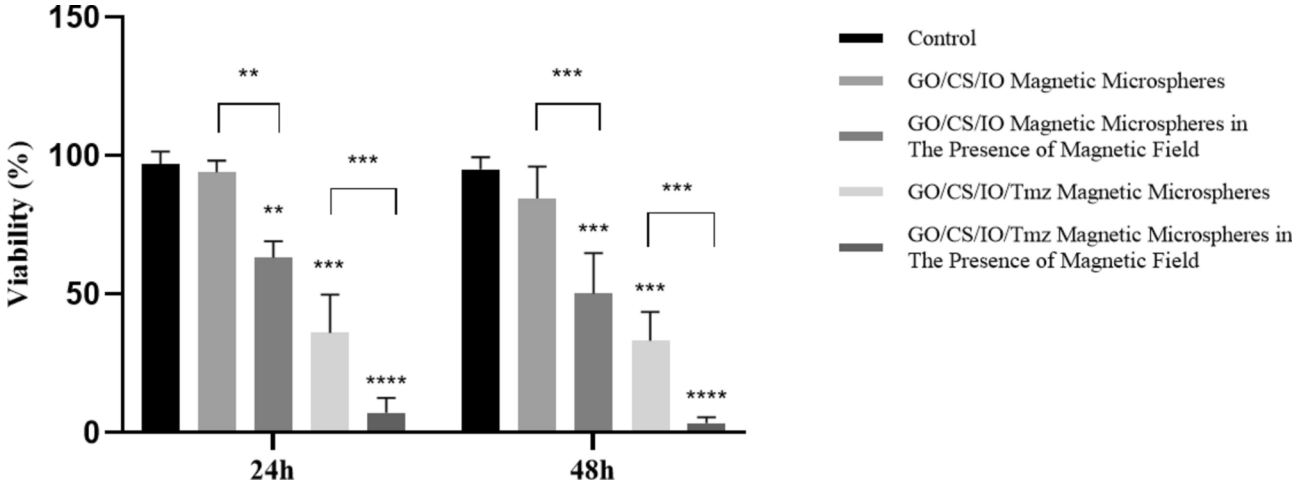

Fig. 9. In vitro cell viability of T98 cell line incubated with (**a**) GO/CS/IO magnetic microspheres, (**b**) GO/CS/IO magnetic microspheres in the presence of magnetic field, (**c**) GO/CS/IO/TMZ magnetic microspheres, (**d**) GO/CS/IO/TMZ magnetic microspheres in the presence of magnetic field, for 24 h (SD ± 2%) and 48 h. $^{*}P < 0.05$, $^{**}P < 0.01$, $^{***}P < 0.001$, $^{****}P < 0.0001$.

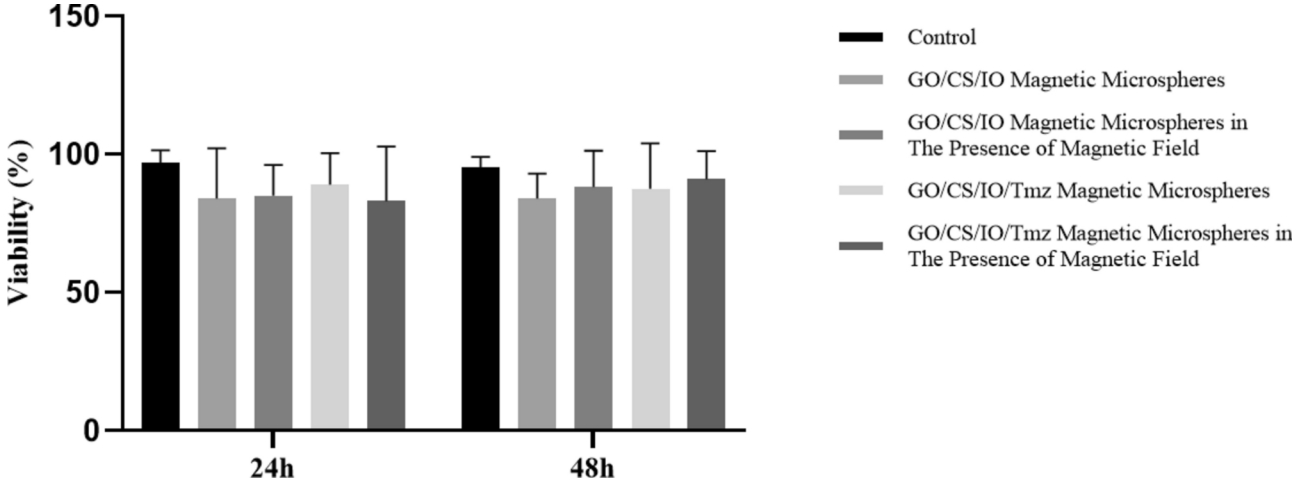

Fig. 11. In vitro cell viability of L929 cell line incubated with (**a**) GO/CS/IO magnetic microspheres, (**b**) GO/CS/IO magnetic microspheres in the presence of magnetic field, (**c**) GO/CS/IO/TMZ magnetic microspheres, (**d**) GO/CS/IO/TMZ magnetic microspheres in the presence of magnetic field, for 24 h (SD ± 2%) and 48 h.

a magnetic field results in a marked decrease in cell viability ($P < 0.01$ for 24 h and $P < 0.001$ for 48 h). Conversely, exposure to a magnetic field significantly reduces cell viability compared to the untreated control group ($P < 0.001$ for 24 h and $P < 0.0001$ for 48 h) and also compared to the group not exposed to the magnetic field ($P < 0.05$ for 24 h and $P < 0.01$ for 48 h). In the case of T98 cells, as illustrated in Figs. 9 and Figs. 10(e–f), the proximity of GO/CS/IO magnetic microspheres in the absence of a magnetic field does not significantly affect cell viability compared to the untreated control group. However, proximity in the presence of a magnetic field leads to a significant decrease in viability ($P < 0.01$ for 24 h and $P < 0.001$ for 48 h). Similarly, for GO/CS/IO magnetic microspheres containing temozolomide, the absence of magnetization results in decreased survival compared to the untreated control group ($P < 0.001$). Exposure to a magnetic field, however, significantly decreases survival compared to both the untreated control group ($P < 0.0001$) and the group not exposed to the magnetic field ($P < 0.001$). The GO/CS/IO microspheres, both with and without temozolomide loading, demonstrated negligible cytotoxic effects on normal fibroblast L929 cells. This lack of significant cytotoxicity was observed consistently, regardless of the presence or absence of an external magnetic field. (Fig. 11). Like in our study, Kun Fang and his team developed doxorubicin-loaded magnetic PLGA microspheres (DOX-MMS) for cancer therapy. The system encapsulates doxorubicin (DOX) within a core, while γ-Fe_2O_3NPs (IOs) are electrostatically assembled on the surface. This configuration ensures high sensitivity to an external alternating current magnetic field (ACMF). The IOs within the PLGA shell induce a thermal effect, enhancing shell permeability and facilitating drug release when activated by ACMF. Experimental results show that DOX-MMS exposed to ACMF for 30 min (21.6%) is

significantly higher than DOX-MMS not exposed (2.8%). This synergistic effect promotes apoptosis in vitro in 4T1 breast cancer cells and effectively inhibits tumor growth in 4T1 tumor xenografts, making DOX-MMS a potent delivery system for efficient magnetic-responsive drug release and combined chemo-thermal therapy[64]. In another research, Shi et al. investigated the cytotoxicity of co-loaded PLGA microspheres containing TMZ and aspirin in human glioma cell lines U-87 and LN229. They found that TMZ-loaded microspheres showed more anti-cancer effectiveness than aspirin-loaded microspheres, decreasing cell proliferation and apoptosis. Aspirin decreased β-catenin transactivation, enhancing TMZ's anti-cancer activity. The co-loaded microspheres may be used to treat GB[65]. Similarly, Zhu and colleagues synthesized PLGA microspheres-BCNU loaded with bis-chloroethyl nitrosourea (BCNU) and studied their impact on GL261 murine glioma cells. The MST of treated cells significantly varied from untreated controls. The inhibitory impact was evident in reduced tumor sizes and decreased expression of the anti-apoptotic protein Bcl-2. Also, Chen et al. developed a formulation for biodegradable PLGA microspheres filled with carboplatin (CBP) for intracerebral administration. The formulation produced significant amounts of CBP at tumor locations without adverse effects. The phagocytic inflammatory response was observed in rat glioma models, with elevated amounts of CBP in tumors. The local administration of PLGA microsphere-CBP increased malignant glioma animals' mean survival time (MST), reduced toxicities, and created large concentrations of CBP at tumor sites[66].

Synthetic or adaptable microspheres have demonstrated potential in controlling drug release when an alternating magnetic field is applied[67]. The magnetic field also enhanced the rate of drug release. The MTT assay results, obtained in the presence and absence of a magnetic field, suggest that the GO/CS/IO/TMZ magnetic microspheres show promise for use in anti-cancer applications due to their effectiveness.

Conclusion

In summary, GO/CS/IO/TMZ magnetic microspheres were created using a straightforward and rapid in situ loading technique. These magnetic microspheres were successfully developed and examined through various methods. They exhibited considerable drug-release characteristics. Moreover, the GO/CS/IO/TMZ magnetic microspheres demonstrated potential magnetic properties that could be utilized for magnetically targeted and pH-responsive drug delivery platforms. The release rate showed a significant difference between a pH of 4.5 and 7.4, suggesting that an acidic microenvironment indicated importance for drug release. The treatment of A172 and T98 cells for 24 and 48 h with the temozolomide-loaded GO/CS/IO nanocomposite, both in the presence and absence of a magnetic field, significantly reduced cell viability compared to the untreated control group. Notably, a significant difference was observed between the groups exposed to the magnetic field and those not, with exposure to the magnetic field further reducing survival. The release of the loaded medicine can be considerably improved by the magnetic response of drug carriers with different magnetic frequencies and intensities.

Data availability

The data would be available from the corresponding author upon reasonable request.

Received: 11 March 2024; Accepted: 19 November 2024
Published online: 02 December 2024

References

1. Silantyev, A. S. et al. Current and future trends on diagnosis and prognosis of glioblastoma: from molecular biology to proteomics. *Cells.* **8**(8), 863 (2019).
2. Rong, L., Li, N. & Zhang, Z. Emerging therapies for glioblastoma: current state and future directions. *Journal of Experimental & Clinical Cancer Research.* **41**(1), 142 (2022).
3. Yeini, E. et al. Targeting Glioblastoma: Advances in Drug Delivery and Novel Therapeutic Approaches. *Advanced Therapeutics.* **4**(1), 2000124 (2021).
4. McKinnon C, Nandhabalan M, Murray SA, Plaha P. Glioblastoma: clinical presentation, diagnosis, and management. Bmj. 2021;374.
5. Sinha, R., Stephenson, J. M. & Price, S. J. A systematic review of cognitive function in patients with glioblastoma undergoing surgery. *Neuro-Oncology Practice.* **7**(2), 131–142 (2020).
6. Tykocki T, Eltayeb M. Ten-year survival in glioblastoma. A systematic review. Journal of Clinical Neuroscience. 2018;54:7–13.
7. Tan AC, Ashley DM, López GY, Malinzak M, Friedman HS, Khasraw M. Management of glioblastoma: State of the art and future directions. CA: a cancer journal for clinicians. 2020;70(4):299–312.
8. Vaz-Salgado, M. A. et al. Recurrent glioblastoma: a review of the treatment options. *Cancers.* **15**(17), 4279 (2023).
9. Strobel, H. et al. Temozolomide and other alkylating agents in glioblastoma therapy. *Biomedicines.* **7**(3), 69 (2019).
10. Aminu, N. et al. The influence of nanoparticulate drug delivery systems in drug therapy. *Journal of drug delivery science and technology.* **60**, 101961 (2020).
11. Abaszadeh F, Ashoub MH, Amiri M. Nanoemulsions challenges and future prospects as a drug delivery system. Current trends in green nano-emulsions: food, agriculture and biomedical sectors. 2023:217–43.
12. Laffleur, F. & Keckeis, V. Advances in drug delivery systems: Work in progress still needed?. *Int J Pharm X.* **2**, 100050 (2020).
13. Adepu S, Ramakrishna S. Controlled Drug Delivery Systems: Current Status and Future Directions. Molecules. 2021;26(19).
14. Ganipineni, L. P., Danhier, F. & Préat, V. Drug delivery challenges and future of chemotherapeutic nanomedicine for glioblastoma treatment. *Journal of controlled release.* **281**, 42–57 (2018).
15. Abaszadeh, F., Ashoub, M. H., Khajouie, G. & Amiri, M. Nanotechnology development in surgical applications: recent trends and developments. *European Journal of Medical Research.* **28**(1), 537 (2023).
16. Liu, J. F., Jang, B., Issadore, D. & Tsourkas, A. Use of magnetic fields and nanoparticles to trigger drug release and improve tumor targeting. *Wiley Interdiscip Rev Nanomed Nanobiotechnol.* **11**(6), e1571 (2019).
17. Gholami, A. et al. Current trends in chemical modifications of magnetic nanoparticles for targeted drug delivery in cancer chemotherapy. *Drug metabolism reviews.* **52**(1), 205–224 (2020).
18. Ashoub, M. H., Amiri, M. & Khajouei, G. *Fe3O4-based nanofluids* 101–127 (Elsevier, 2024).

19. Ashoub, M. H., Razavi, R., Heydaryan, K., Salavati-Niasari, M. & Amiri, M. Targeting ferroptosis for leukemia therapy: exploring novel strategies from its mechanisms and role in leukemia based on nanotechnology. *European Journal of Medical Research.* **29**(1), 224 (2024).
20. Anjum, T. et al. Magnetic nanomaterials as drug delivery vehicles and therapeutic constructs to treat cancer. *Journal of Drug Delivery Science and Technology.* **80**, 104103 (2023).
21. Anwer AH, Ahtesham A, Shoeb M, Mashkoor F, Ansari MZ, Zhu S, et al. State-of-the-art advances in nanocomposite and bio-nanocomposite polymeric materials: A comprehensive review. Advances in Colloid and Interface Science. 2023:102955.
22. Roy, M., Roy, A., Rustagi, S. & Pandey, N. An overview of nanomaterial applications in pharmacology. *BioMed Research International.* **2023**(1), 4838043 (2023).
23. Sharma, H. & Mondal, S. Functionalized graphene oxide for chemotherapeutic drug delivery and cancer treatment: a promising material in nanomedicine. *International Journal of Molecular Sciences.* **21**(17), 6280 (2020).
24. Itoo, A. M. et al. Multifunctional graphene oxide nanoparticles for drug delivery in cancer. *Journal of Controlled Release.* **350**, 26–59 (2022).
25. Guo, Z. et al. Surface functionalization of graphene-based materials: Biological behavior, toxicology, and safe-by-design aspects. *Advanced Biology.* **5**(9), 2100637 (2021).
26. Ghulam, A. N. et al. Graphene oxide (GO) materials—Applications and toxicity on living organisms and environment. *Journal of Functional Biomaterials.* **13**(2), 77 (2022).
27. Schubert, J. & Chanana, M. Coating matters: Review on colloidal stability of nanoparticles with biocompatible coatings in biological media, living cells and organisms. *Current medicinal chemistry.* **25**(35), 4553–4586 (2018).
28. Singh, D. P. et al. Graphene oxide: An efficient material and recent approach for biotechnological and biomedical applications. *Materials Science and Engineering: C.* **86**, 173–197 (2018).
29. Jain, V. P. et al. Advanced functionalized nanographene oxide as a biomedical agent for drug delivery and anti-cancerous therapy: a review. *European Polymer Journal.* **142**, 110124 (2021).
30. Leitao, M. M. et al. Sulfobetaine methacrylate-functionalized graphene oxide-IR780 nanohybrids aimed at improving breast cancer phototherapy. *RSC advances.* **10**(63), 38621–38630 (2020).
31. Wang, W., Xue, C. & Mao, X. Chitosan: Structural modification, biological activity and application. *International Journal of Biological Macromolecules.* **164**, 4532–4546 (2020).
32. Mikušová, V. & Mikuš, P. Advances in chitosan-based nanoparticles for drug delivery. *International Journal of Molecular Sciences.* **22**(17), 9652 (2021).
33. Zhang, X. et al. Development and characterization of size controlled polymeric microcapsules loaded with superparamagnetic nanoparticles. *Polymer composites.* **34**(4), 443–449 (2013).
34. Gurung, B. D. & Kakar, S. An overview on microspheres. *Int J Health Clin Res.* **3**(1), 11–24 (2020).
35. Patil, N., Wadd, N., Thorat, S. & Upadhye, S. Microspheres: A novel drug delivery system. *Am J PharmTech Res.* **10**(02), 286–301 (2020).
36. Su, Y. et al. PLGA-based biodegradable microspheres in drug delivery: recent advances in research and application. *Drug delivery.* **28**(1), 1397–1418 (2021).
37. Amiri, M., Khazaeli, P., Salehabadi, A. & Salavati-Niasari, M. Hydrogel beads-based nanocomposites in novel drug delivery platforms: Recent trends and developments. *Advances in Colloid and Interface Science.* **288**, 102316 (2021).
38. Amiri, M., Akbari, A., Ahmadi, M., Pardakhti, A. & Salavati-Niasari, M. Synthesis and in vitro evaluation of a novel magnetic drug delivery system; proecological method for the preparation of CoFe2O4 nanostructures. *Journal of Molecular Liquids.* **249**, 1151–1160 (2018).
39. Oalđe Pavlović, M. et al. A study of phytochemistry, genoprotective activity, and antitumor effects of extracts of the selected Lamiaceae species. *Plants.* **10**(11), 2306 (2021).
40. Bodnar Willard MA, McGuffin VL, Waddell Smith R. Forensic analysis of Salvia divinorum using multivariate statistical procedures. Part I: discrimination from related Salvia species. Analytical and bioanalytical chemistry. 2012;402:833–42.
41. Capek P, Hřibalová V. Water-soluble polysaccharides from Salvia officinalis L. possessing immunomodulatory activity. Phytochemistry. 2004;65(13):1983–92.
42. Staudenmaier, L. Verfahren zur darstellung der graphitsäure. *Berichte der deutschen chemischen Gesellschaft.* **31**(2), 1481–1487 (1898).
43. Ashoub, M. H. et al. Induction of ferroptosis cell death in acute promyelocytic leukemia cell lines (NB4 and HL-60) using hydrothermally synthesized ZnO NPs in the presence of black cardamom extract. *Results in Engineering.* **20**, 101479 (2023).
44. Taeby, M., Ashoub, M. H., Asghari, M., Farsinejad, A. & Amiri, M. Sol–gel synthesis of strontium ferrate (SrFeO3) nanoparticles and evaluation of anti-leukemic effects against leukemic cell lines. *Journal of Sol-Gel Science and Technology.* **109**(1), 56–65 (2024).
45. Katoueezadeh, M. et al. Combinatorial targeting of telomerase and DNA-PK induces synergistic apoptotic effects against Pre-B acute lymphoblastic leukemia cells. *Molecular Biology Reports.* **51**(1), 163 (2024).
46. Yari F, Ashoub MH, Amirizadeh N, Nikougoftar M, Valandani HM, Khalilabadi RM. Differential Expression of the hTERT Gene in Umbilical Cord-Derived Mesenchymal Stem Cells Cocultured with B Cell Precursor Leukemia Cell Microparticles or CD41+/CD61+ Platelet Microparticles. Biochemical Genetics. 2023:1–14.
47. Ashoub MH, Amiri M, Fatemi A, Farsinejad A. Evaluation of ferroptosis-based anti-leukemic activities of ZnO nanoparticles synthesized by a green route against Pre-B acute lymphoblastic leukemia cells (Nalm-6 and REH). Heliyon. 2024;10(17).
48. Dutta, B. et al. Surface engineered Fe 3 O 4 nanomagnets for pH-responsive delivery of gemcitabine hydrochloride and in vivo tracking by radiolabeling. *Materials Advances.* **4**(1), 195–204 (2023).
49. Mohassel, R. et al. Pechini synthesis using propylene glycol and various acid as stabilizing agents and characterization of Gd2NiMnO6 ceramic nanostructures with good photocatalytic properties for removal of organic dyes in water. *Journal of Materials Research and Technology.* **9**(2), 1720–1733 (2020).
50. Khobragade, P. S., Hansora, D. P., Naik, J. B., Njuguna, J. & Mishra, S. Physico-mechanical properties of nano-polystyrene-decorated graphene oxide–epoxy composites. *Polymer international.* **66**(10), 1402–1409 (2017).
51. Do Kim, K., Kim, S. S., Choa, Y.-H. & Kim, H. T. Formation and surface modification of Fe3O4 nanoparticles by co-precipitation and sol-gel method. *Journal of Industrial and Engineering Chemistry.* **13**(7), 1137–1141 (2007).
52. Khobragade, P. S., Hansora, D., Naik, J. B., Njuguna, J. & Mishra, S. Preparation and analysis of multi-layered hybrid nanostructures. *Applied clay science.* **132**, 668–674 (2016).
53. Brück S. Magnetic resonant reflectometry on exchange bias systems. 2009.
54. Manginas G. Heat Assisted Magnetic Recording using Exchange Bias: University of York; 2020.
55. Teichert N, Boehnke A, Behler A, Weise B, Waske A, Hütten A. Exchange bias effect in martensitic epitaxial Ni-Mn-Sn thin films applied to pin CoFeB/MgO/CoFeB magnetic tunnel junctions. Applied Physics Letters. 2015;106(19).
56. Zhang Y, Huang L-j, Wang Y-x, Tang J-g, Wang Y, Cheng M-m, et al. The preparation and study of ethylene glycol-modified graphene oxide membranes for water purification. Polymers. 2019;11(2):188.
57. Ahmed TA, Aljaeid BM. Preparation, characterization, and potential application of chitosan, chitosan derivatives, and chitosan metal nanoparticles in pharmaceutical drug delivery. Drug design, development and therapy. 2016:483–507.
58. Walke, S. et al. Fabrication of chitosan microspheres using vanillin/TPP dual crosslinkers for protein antigens encapsulation. *Carbohydrate polymers.* **128**, 188–198 (2015).

59. Shah, U., Joshi, G. & Sawant, K. Improvement in antihypertensive and antianginal effects of felodipine by enhanced absorption from PLGA nanoparticles optimized by factorial design. *Materials Science and Engineering: C.* **35**, 153–163 (2014).
60. Mustapić, M. et al. Controlled delivery of drugs adsorbed onto porous Fe3O4 structures by application of AC/DC magnetic fields. *Microporous and Mesoporous Materials.* **226**, 243–250 (2016).
61. Raj H, Sharma S, Sharma A, Verma KK, Chaudhary A. A novel drug delivery system: Review on microspheres. Journal of Drug Delivery and Therapeutics. 2021;11(2-S):156–61.
62. Dhamapurkar, S. P. & Desai, D. M. A review on microsphere for novel drug delivery system. *World Journal of Advanced Research and Reviews.* **16**(3), 529–538 (2022).
63. Duwa, R., Emami, F., Lee, S., Jeong, J.-H. & Yook, S. Polymeric and lipid-based drug delivery systems for treatment of glioblastoma multiforme. *Journal of Industrial and Engineering Chemistry.* **79**, 261–273 (2019).
64. Fang, K. et al. Magnetic field activated drug release system based on magnetic PLGA microspheres for chemo-thermal therapy. *Colloids and Surfaces B: Biointerfaces.* **136**, 712–720 (2015).
65. Shi, Z. D. et al. Aspirin-/TMZ-coloaded microspheres exert synergistic antiglioma efficacy via inhibition of β-catenin transactivation. *CNS Neurosci Ther.* **19**(2), 98–108 (2013).
66. Zhu, T. et al. BCNU/PLGA microspheres: a promising strategy for the treatment of gliomas in mice. *Chin J Cancer Res.* **26**(1), 81–88 (2014).
67. Mertz D, Sandre O, Begin-Colin S. Drug releasing nanoplatforms activated by alternating magnetic fields. Biochimica et Biophysica Acta (BBA)-General Subjects. 2017;1861(6):1617–41.

Acknowledgements

The authors are grateful to the Council of Neuroscience Research Center, Institute of Neuropharmacology, and Kerman University of Medical Science for financial support in undertaking this work.

Author contributions

Meysam Ahmadi: Investigation, Writing- Original draft preparation, Visualization, Methodology. Muhammad Hossein Ashoub: Methodology, Resources, Formal Analysis, Writing- Reviewing and Editing. Kamran Heydarian: Resources, Writing- Reviewing and Editing. Sanaz Abolghasemi: Methodology, Writing- Reviewing and Editing. Elmuez A. Dawi: Methodology, Writing- Reviewing and Editing. Ghazal khajouei: Methodology, Writing- Reviewing and Editing. Mahnaz Amiri: Conceptualization, Supervision, Methodology, Validation, Writing-Reviewing and Editing.

Funding

This study was supported by grant No. 401000014 from the Kerman University of Medical Sciences.

Declarations

Competing interests

The authors declare no competing interests.

Ethics approval and consent to participate

The study gained the approval of the ethical committee of the Kerman University of Medical Sciences. All methods were performed following the relevant guidelines and regulations.

Additional information

Correspondence and requests for materials should be addressed to G.k. or M.A.